Thermochimica Acta 502 (2010) 51–59

Contents lists available at ScienceDirect

Thermochimica Acta

journal homepage: www.elsevier.com/locate/tca

Mesomorphic properties of (*S*)-MHPSBO*n* series

Mirosława D. Ossowska-Chruściel*, J. Chruściel

Institute of Chemistry, University of Podlasie, 3-go Maja 54, 08-110 Siedlce, Poland

ARTICLE INFO

Article history:
Received 3 August 2009
Received in revised form
29 December 2009
Accepted 3 February 2010
Available online 10 February 2010

Keywords:
Chiral liquid crystals
Smectic phases
Ferroelectric and antiferroelectric phases
Spontaneous polarization
Mesomorphic and electro-optic properties
DSC calorimetry
POM
TLI and X-ray measurements

ABSTRACT

This article reports new results on synthesis and mesomorphic properties of the homologous series of (*S*)-1-methylheptyl-4-(4′-alkyloxybiphenylthiocarboxy)-benzoates, referred to as (*S*)-MHPSBO*n*, where *n* varies from 7 to 10 and denotes the number of carbon atoms in the alkyl chain. These compounds are sulphur analogous to a liquid crystal known as MHPOBC, where the central ester bridge was replaced with the –COS– connecting group. The (*S*)-MHPSBO*n* homologous series possesses enantiotropic SmA*, SmC*, SmC^*_A and monotropic SmI* phases for $n = 7–10$. The (*S*)-MHPSBO7 compound has also smectic chiral subphases: SmC^*_α and SmC^*_γ. Their mesomorphic properties were investigated by means of polarizing optical microscopy (POM), differential scanning calorimetry (DSC), transmittance light intensity (TLI), X-ray diffraction and electro-optic (EO) measurements.

1. Introduction

The antiferroelectric order in liquid crystals was first observed in 4-(1-methylheptyloxycarbonyl)phenyl-4′-octyloxybiphenyl-4-carboxylate in compound well known as MHPOBC in 1989 [1] and since then is the subject of intensive investigations (see e.g. [2–9]).

The high optical purity MHPOBC is characterized by antiferroelectric SmC^*_A, paraelectric SmA* and three chiral subphases: SmC^*_α, SmC^*_γ and SmC^*_β between SmA* and SmC^*_A phases. The chiral subphases are observed for high optical purity (*S*)-MHPOBC or (*R*)-MHPOBC isomers only. The SmC^*_β subphase is not observed when one enantiomer contains 1.5% second. In this case, the sequence of $SmC^*_\alpha \leftrightarrow SmC^* \leftrightarrow SmC^*_\gamma \leftrightarrow SmC^*_A$ phases is observed. The SmC^*_γ subphase disappears when an admixture of one enantiomer is higher than 5.6%. The SmC^*_α is not present in a racemic mixture [8].

After antiferroelectric properties of MHPOBC were discovered, many chiral compounds exhibiting the antiferroelectric phases have been synthesized in the past several years [9–12] and the influence of different chemical structures on the phase polymorphism has been studied. In particular, the influence of thioester linking group on the stabilization of SmC phase in chiral and achiral compounds is a well-known phenomenon [13–20].

Among the constituents of liquid crystals core, ester and thioester groups are listed among the most important links. A thioester group often improves thermal stability of the mesophases. It has been well known that many achiral liquid crystals having a thioester linkage tend to exhibit smectic phases, namely SmC and SmA. Chiral thioester materials described in this article, particularly homologue $n = 7$, seem to be interesting as mesogens forming intermediate ferro- and antiferroelectric SmC* phases and having a sulphur atom in a rigid core are rare, but, considering their practical applications, very much desired.

In what follows, a convenient and efficient method of synthesis will be given and the properties of four chiral liquid crystal compounds belonging to a new homologous series of chiral thiobenzoates, $C_nH_{2n+1}O–Ph–Ph–COS–Ph–COO–C^*H(CH_3)C_6H_{13}$, abbreviated to as (*S*)-MHPSBO*n* (*n* varies from 7 to 10 and denotes the number of carbon atoms in the alkoxy chain) will be presented. In these compounds the 4-alkoxybiphenyl is connected with –COS– central group and the chiral branched chain in (*S*)-4-(1-methylheptyloxycarbonyl)phenyl is attached to the thioester central group in the *p*-position. The phase polymorphism compounds from (*S*)-MHPSBO*n* homologous series were investigated by means of three complementary methods: POM, DSC and TLI. X-ray diffraction and electro-optic (EO) studies were also carried out. The phase situation was characterized by means dielectric spectroscopy as well [21]. A strong influence of alkoxy group on the sequence of phases was observed.

* Corresponding author. Tel.: +48 25 6431010.
E-mail address: dch@ap.siedlce.pl (M.D. Ossowska-Chruściel).

0040-6031/$ – see front matter © 2010 Elsevier B.V. All rights reserved.
doi:10.1016/j.tca.2010.02.006

2. Experimental

2.1. Characterization

The structures of the intermediate and final compounds were confirmed by elemental analysis (EA), IR, ^{1}H NMR, ^{13}C NMR and MS spectroscopic methods. IR spectra were recorded on a FTIR Nicolet Magna 760 spectrometer using a minimum of 64 co-added scans at a resolution of 1 cm^{-1}. The NMR spectra were obtained with a Varian Unity Plus spectrometer operating at 500 MHz ($CDCl_3$, TMS as internal standard). MS spectra were obtained by MS TOF ES+. The chemical purity was checked by thin layer chromatography (TLC) and further confirmed by elemental analysis using a Perkin-Elmer 2400 spectrometer. The optical purity of the compounds was determined by chiral HPLC and ^{13}C NMR. Transitions temperatures were examined by polarized optical microscopy (POM), transmitted light intensity (TLI) and differential scanning calorimetry (DSC). Heating and cooling rates for all POM, TLI and DSC measurements were the same (±0.5 and ±2.0 °C min^{-1}). The temperature was controlled with a Linkam controller with an accuracy of ±0.1 °C (Linkam programmable heating stage THMSE 600 was used). Our TLI measuring set was further described in [22]. DSC measurements were performed using a DSC 822^e Mettler Toledo Star System differential scanning calorimetry. The examinations of POM and TLI were done on planar aligned samples, using AWAT electro-optic cells, type of HG cell, 6.4 μm thick (a trade mark of electro-optic cells made by AWAT Company, Poland) with ITO electrodes. Measurements of the polarization reversal current were performed according to the well-known triangular-wave technique. X-ray investigations were performed on a Philips X'Pert diffractometer as well as on a Guinier symmetrical focusing transmission photographic camera. The analysis of TG, DTG and DTA curves obtained for compounds from the (*S*)-MHPSBO*n* homologous series (by repeatedly heating and cooling the sample from crystalline to isotropic phases) confirmed the high thermal stability of investigated liquid crystals.

2.2. Preparation of materials

The chemical structure of chiral mesogens from the (*S*)-MHPSBO*n* homologous series is presented in Fig. 1.

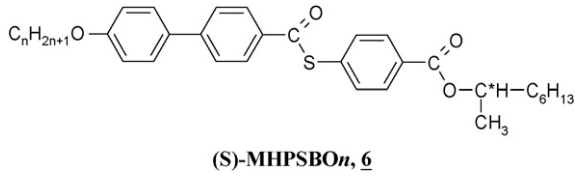

(S)-MHPSBO*n*, 6

Fig. 1. Chemical structure of mesogens from the (*S*)-MHPSBO*n* homologous series.

The method applied earlier was based on the reaction of chlorides of 4-alkoxybiphenyl-carboxylic acid with 4-mercaptobenzoic acid. The similar method of (*S*)-MHPSBO8 synthesis was previously described in paper [9]. This method leads up to obtaining low yields of higher homologous.

Taking into consideration the high vulnerability of 4-mercaptobenzoic acid to create sulfide and disulfide bonds and therefore small chemical yields of 4-[4-(4′-alkoxybiphenyl)carbonylthio]benzoic acids, a new method of synthesis was developed. Compounds from the (*S*)-MHPSBO*n* series were prepared according to following the procedures presented in detail in Fig. 2. The synthesis of the homologous series of mesogens described by formula **6** was carried out with the use of 4-mercaptobenzoic acid **1**.

Our new method (Fig. 2) is an innovation and a considerable improvement with respect to what has been presented previously [9]. 4′-(4-Alkoxybiphenyl)carboxylic acid (*n*OBB with *n* from 7 to 10) and (*S*)-1-methylheptyl 4-mercaptobenzoate (**4**, (*S*)-MHCBSH) were used as intermediate products. The *n*OBB acids were obtained using the modified Williamson method [23]. Under slow oxidation 4-mercaptobenzoic acid **1** was transformed into dithiodibenzoic acid. The acid chloride (**2** and **5**, Fig. 2) was obtained by means of the usual method. The (*S*)-1-methylheptyl 4,4′-dithiodibenzoates **3** (Fig. 2) was obtained by the esterification of **2** with the (*S*)-2-octanol in the presence of pyridine and CH_2Cl_2. The (*S*)-2-octanol was purchased from Fluka Co. Chem., chiral select 99.5%. The compound **3** was reduced with sodium borohydride in absolute ethanol under nitrogen. The final compounds (*S*)-MHPSBO*n* **6** were obtained by the esterification of **4** and 4-alkyloxybiphenyl-carboxylic acid chloride **5** with 72–76% yield. All compounds, intermediate and final,

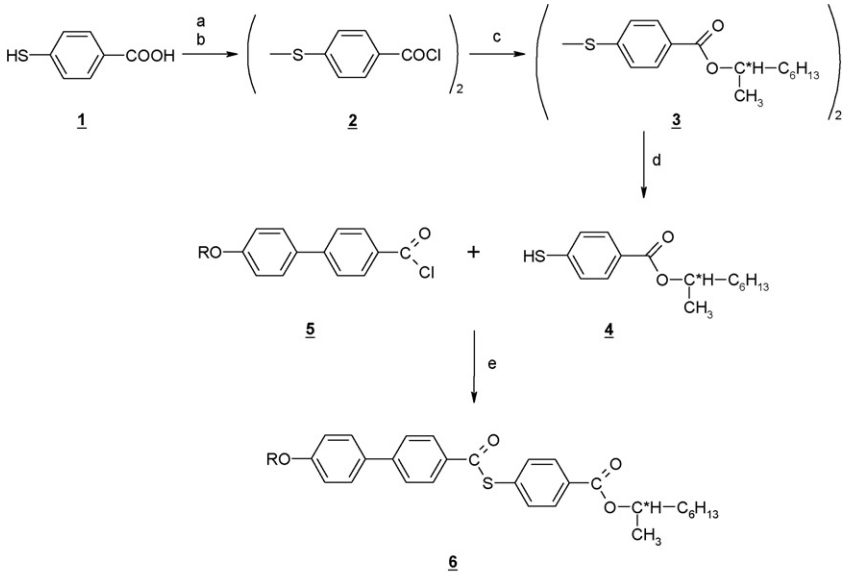

R: -C_nH_{2n+1}; a: $NaOH_{aq}$, I_2; b: $SOCl_2$; c: (*S*)-2-octanol, pyridine, toluene;
d: $NaBH_4$, EtOH abs., N_2; e: toluene, piridine

Fig. 2. A convenient preparation of new chiral of thiobenzoate from the (*S*)-MHPSBO*n* homologous series.

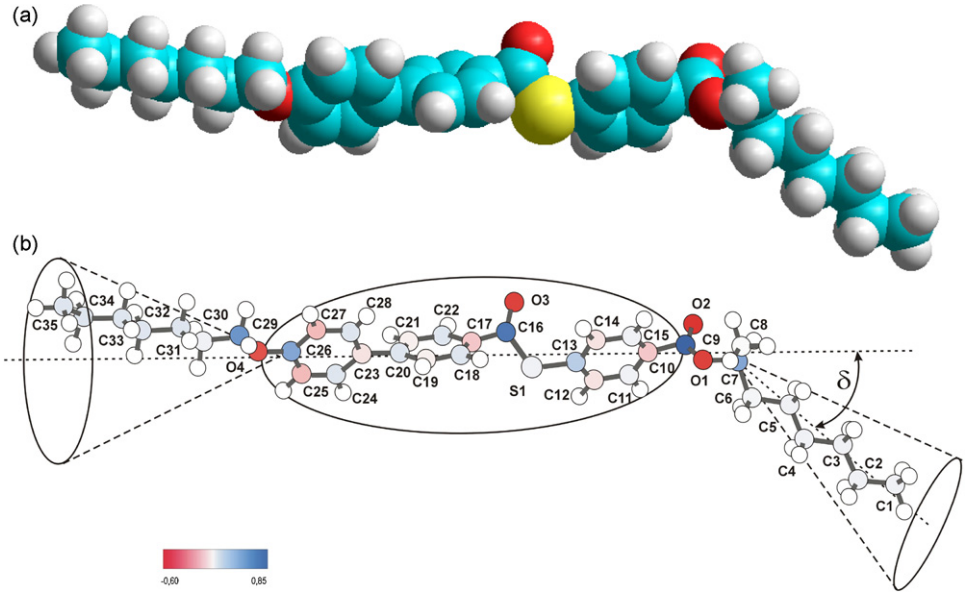

Fig. 3. Molecular configuration of the (*S*)-MHPSBO*n*: (a) molecular model of the (*S*)-MHPSBO7 compound and (b) postulated molecular configuration.

were purified by column chromatography and crystallization until their melting point was constant. The optical purity of all homologous was checked by chiral HPLC and also ^{13}C NMR method of comparative measurements. ^{13}C NMR method is one of methods applied to determine for optical purity (enantiomer contains). The samples of (*S*)-MHPSBO*n* showed the formation of desired (*S*)-**6** with 99.5% ± 0.1 ee with respect to the starting compound (*S*)-2-octanol.

2.2.1. Preparation of compound (S)-MHCBSH-4

40 ml thionyl chloride was added to the suspension of 4,4′-dithiodibenzoic acid (4.77 g, 15 mmol) in anhydrous toluene (40 ml). The mixture was refluxed until the dissolution was complete. The mixture was extracted with hot hexane and then concentrated. The crude product was then crystallized from the hexane. 4,4′-Dithiodibenzoyl chloride **2** (m.p. 80–82 °C) was obtained with 73% yield. ^1H NMR (500 MHz, $CDCl_3$); δ (ppm); 8.05 (m, 4H, *ortho* to –COCl); 7.59 (m, 4H, *ortho* to –S–S–).

The compound **2** (1.72 g, 5 mmol) was dissolved in dry toluene (30 ml), to which 0.45 g (6 mmol) of dry pyridine was added. The solution was stirred for 0.5 h and then 1.54 g (5 mmol) of (*S*)-2-octanol in 30 ml dry toluene was added dropwise. The mixture was stirred at 35–40 °C for 18 h (TLC control, R_f = 0.48 in $CHCl_3$). Then it was filtrated, and the filtrate was washed with cold water with hydrochloric acid and again washed with cold water. The toluene layer was dried over anhydrous magnesium sulfate and concentrated under vacuum to the yellow oil, then purified by column chromatography on silica gel using CH_2Cl_2 as eluent. The product **3** was obtained as light yellow oil (72% yield). ^1H NMR (500 MHz, $CDCl_3$); δ (ppm): 0.86 (t, 6H, $-CH_3$); 1.29 (m, 22H, al); 1.62 (m, 4H, $-CH_2-$); 5.13 (s, 2H to C*); 7.50 (m, 4H, *ortho* to –S–S–); 7.95 (m, 4H, *ortho* to –COO). IR (KBr, cm^{-1}): 1720, 1611, 1509, 445 cm^{-1}.

Portions of sodium borohydride (0.36 g, 10 mmol) were added to the solution of **3** (2.7 g, 5 mmol) in absolute ethanol (70 ml), which was then stirred under nitrogen at RT for 1 h (TLC, R_f of product 0.62 CH_2Cl_2). The reaction mixture was added to water containing ice and hydrochloric acid and extracted with dichloromethane (3 × 50 ml). The combined dichloromethane layers were washed with water, next they were dried ($MgSO_4$), filtrated, then dry silica gel (2 g) was added to them and they were evaporated to dryness. The silica gel plug was placed on top of chromatography column and eluted with CH_2Cl_2 under dry argon. The product **4** was obtained as hell oil with 68% yield. The optical purity was 99.5 ± 0.1% (HPLC). ^1H NMR (500 MHz, $CDCl_3$), δ (ppm): 0.98 (t, 3H, $-CH_3$); 1.39 (m, 11H, alkyl); 1.75 (m, 2H, $-C^*-CH_2$); 3.72 (s, 1H, –SH); 5.18 (s, 1H, –C*H–); 7.10 (d, 2H–Ar *ortho* to –SH), 7.95 (d, 2H–Ar *ortho* to –COOR). IR (KBr, cm^{-1}): 2570 (SH), 1680 (COO), 1600 (phenyl ring stretching). EA (%) calc. for $C_{15}H_{22}O_2S$: C 67.67, H 8.27, S 12.03; found C 67.70, H 8.23, S 12.00.

2.2.2. General procedure for the preparation of compound (S)-MHPSBOn

Details for (*S*)-MHPSBO7 are given as typical. 11 mmol of dry pyridine was added to the solution (10 mmol) of compound 5 in 50 ml of dry toluene and then stirred for 30 min. Next, the solution of 10 mmol compound **4** in 50 ml of dry toluene was added to the mixture. The reaction mixture was stirred for 12–15 h at 35–45 °C. When the analysis by TLC revealed a complete reaction, the reaction mixture was cooled to 10 °C and added to water containing ice and hydrochloric acid (10 ml, 15%). The organic layer was washed several times with water and an aqueous solution of sodium carbonate. The organic phases were dried over anhydrous magnesium sulphate and then filtrated. The filtrated solvent was evaporated. The residue was purified by column chromatography on silica gel using CH_2Cl_2 to give a white solid, which was then recrystallized from absolute ethanol to white crystals; m.p. 119.7–120.5 °C. The yield of final compound was 75.6%. ^1H NMR (500 MHz, $CDCl_3$, δ, ppm): 8.08 (2d, J = 8.6, 4H; 2H *ortho* to –COS–, 2H *ortho* to –COO–), 7.60 (m, 6H, 2H *ortho* to $-OCH_2-$, 4H *ortho* to $-C_6H_4-$), 7.00 (d, J = 8.0, 2H, *ortho* to –SCO–), 5.17 (s, J = 6.4, 1H, –C*H–), 4.00 (t, J = 6.6, 2H, $-CH_2-$, α to $-OC_6H_4-$), 1.71 (m, 4H, $-CH_2-$, β to $-OC_6H_4-$ and α to –C*H–), 1.35 (m, 19H, $-CH_2-$), 0.90 (m, 6H, $-CH_3$). ^{13}C NMR (500 MHz, $CDCl_3$, δ, ppm): 188.61 (1C, –COS–), 165.57 (1C, –COO–), 159.88 (1C, C_5H_4C–OR), 146.51 and 133.20 (2C, $-C_5H_4C-CC_5H_4-$), 134.89 (1C, Ar, *ortho* to –OR), 134.51 (1C, C_5H_4C–SCO–), 131.85 (2C, C_5H_4C–CO–), 130.27 (2C, Ar, *meta* to –OR), 128.52 (2C, *meta* to –COS–), 128.30 (2C, *ortho* to –SCO–), 126.88 (2C, *ortho* to –COOR), 115.19 (2C, *ortho* to –COS–), 36.23 (1C*), 31.11–14.56 (13C, alkyl). IR (KBr, cm^{-1}): 2931, 2858, 1714, 1674, 1528 and 1190.

MS (*m*/*z*, %): 560.7 (M^+, 100.00). EA (%) calc. for $C_{35}H_{44}O_4S$: C 75.00, H 7.86, S 5.71; found C 75.07, H 7.80, S 5.70.

Table 1
Phase behaviour of the (*S*)-MHPSBO*n* series obtained during heating and cooling.

(*S*)-MHPSBO*n*	$C_nH_{2n+1}O$–Ph–Ph–COS–Ph–COO–C*H(CH_3)C_6H_{13}	
	Heating	Cooling
(*S*)-MHPSBO7	Cr2 82.1 (19.0), Cr1 117.3 (52.0), SmC_A^* 140.9 (0.02), SmC_γ^* 141.6 (0.04), SmC* 144.8 (0.02), SmC_α^* 145.8 (0.05), SmA* 184.2 (12.3) I	I 184.0 (14.3), SmA* 145.8 (0.05), SmC_α^* 144.8 (0.02), SmC* 141.4 (0.04), SmC_γ^* 140.6 (0.02), SmC_A^* 116.9 (3.3), SmI* 78.1 (32.3), Cr1 71.4 (10.5) Cr2
(*S*)-MHPSBO8	Cr 111.6 (54.6), SmC_A^* 146.1 (0.14), SmC* 151.1 (0.59), SmA* 177.8 (11.5) I	I 177.8 (11.2), SmA* 151.6 (0.53), SmC* 144.4 (0.09), SmC_A^* 107.6 (3.1), SmI* 72.9 (36.5) Cr
(*S*)-MHPSBO9	Cr 96.1 (5.4), SmC_A^* 146.3 (0.06), SmC* 152.2 (0.13), SmA* 168.4 (8.4) I	I 167.9 (7.9), SmA* 151.3 (0.08), SmC* 145.2 (0.05), SmC_A^* 92.9 (0.2), SmI* 49.2 (3.9) Cr
(*S*)-MHPSBO10	Cr 83.1 (56.1), SmC_A^* 144.9 (0.14), SmC* 153.8 (1.03), SmA* 166.1 (9.1) I	I 165.9 (8.7), SmA* 153.4 (1.0), SmC* 142.9 (0.11), SmC_A^* 85.9 (1.4), SmI* 29.6 (26.0) Cr

Transition temperatures (°C) and enthalpies (in parentheses, kJ g^{-1}) were determined from DSC scans at 2 and 0.5 K min^{-1}; Cr denotes crystalline phase, SmC_α^* and SmC_γ^* are chiral subphases, SmC* is chiral ferroelectric phase, SmC_A^* is chiral antiferroelectric phase, SmI* is chiral smectic phase, SmA* and SmB* are orthogonal phases and I is isotropic phase.

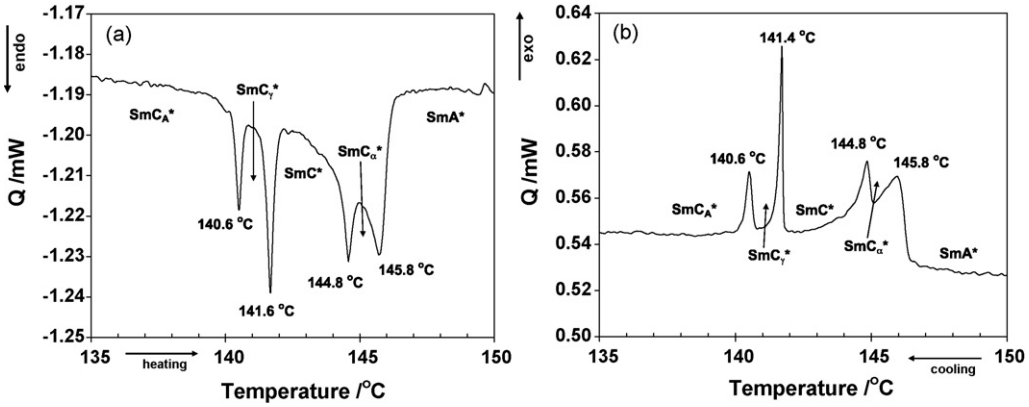

Fig. 4. DSC curve obtained during heating (a) and cooling (b) of (*S*)-MHPSBO7 (±0.5 °C min^{-1}).

3. Results and discussion

A molecular model of (*S*)-MHPSBO*n* (for *n* = 7) is shown in Fig. 3. The all-trans conformation for alkyl and alkoxy chains were found for the molecules of thioester series in the solid state [24–26], however in the liquid and liquid crystalline state many different conformations occur. Theoretical calculations for the investigated molecules were carried out by means of the semi-empirical MINDO3 method. The result is shown in Fig. 3.

The net charge of the (*S*)-MHPSBO*n* molecule shows three dipole groups: –COS– in the central part and two groups, –COOC*H(CH_3)C_6H_{13} and –OR in the terminal chains. The largest negative charges can be found at oxygen atoms O1, O2, O3 and O4, whereas the sulphur atom S1 has a slight positive charge. The chiral end chain is bent by about δ ca. 42° with respect to the core direction. Crystallographic investigations in the crystalline phase of MHPOBC prove that the chiral branched terminal chain and the nearest phenyl plane are tilted with respect to each other

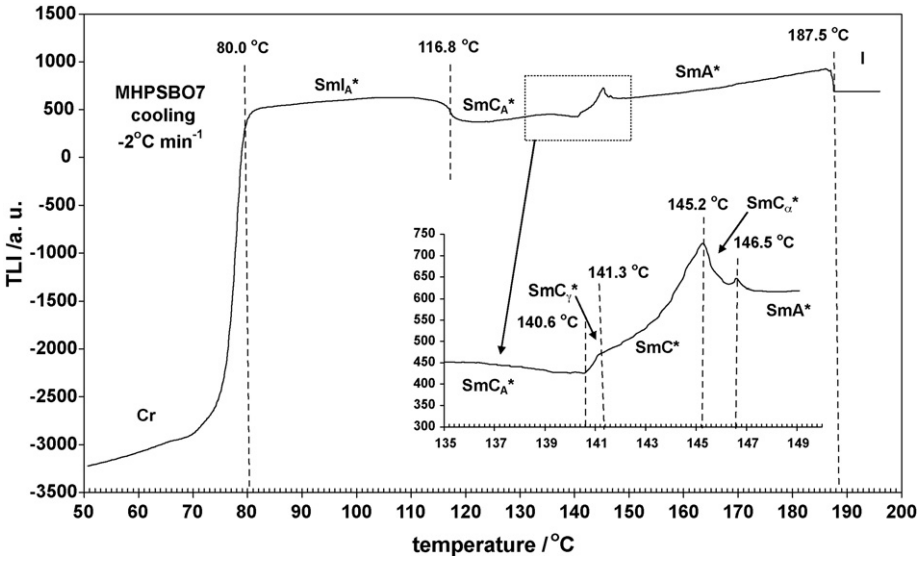

Fig. 5. TLI curve obtained during cooling (−2 °C min^{-1}) of (*S*)-MHPSBO7.

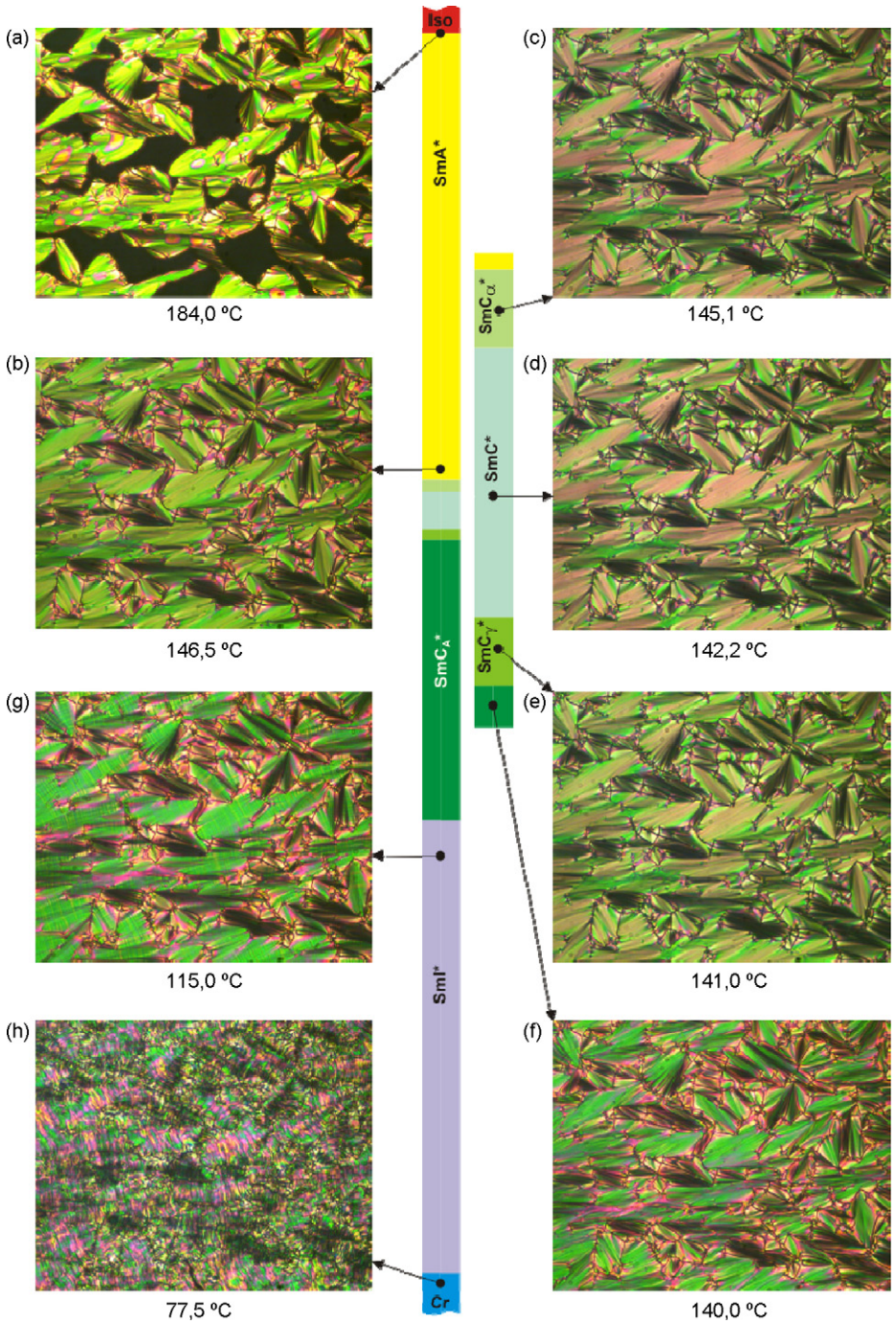

Fig. 6. Textures of the SmA*, SmC$^*_\alpha$, SmC*, SmC$^*_\gamma$, SmC$^*_A$, SmI* and Cr phases observed during cooling of the (*S*)-MHPSBO7.

by ca. 90° [27,28]. It was also confirmed that the molecules are also bent even in the liquid crystalline phase. Polarized FT-IR [29] and NMR [30,31] measurements of MHPOBC suggest that the chiral chain is bent at the magic angle (54.7°) and ca. 43° (^{13}C NMR) or 38–76° (^{2}H NMR) respectively. The results obtained from semi-empirical methods indicate also that the angle between the chiral terminal group (*S*)-1-methylheptyloxy and the nearest phenyl plane is at ca. 90° in 5BoOSMH and 5PhOSMH compounds [16]. The postulated molecular configuration compounds from homologous series of (*S*)-MHPSOB*n*, of MHPOBC analogues are shown in Fig. 3.

Transition temperatures for all compounds obtained during heating and cooling are presented in Table 1.

The enthalpy changes for (*S*)-MHPSBO*n* have been established by DSC investigations and are presented in Table 1. They show that the (*S*)-MHPSBO7 is characterized by rich phase polymorphism: antiferroelectric SmC$^*_A$, ferroelectric SmC* and paraelectric SmA*, as well as two subphases: SmC$^*_\alpha$ between phases SmA* and SmC* and SmC$^*_\gamma$ between SmC$^*_A$ and SmC* and highly ordered tilted SmI* phase. The optical purity was comparable between all compounds (99.5 ± 0.1%), suggests that the presence of smectic chiral subphases is the property of (*S*)-MHPSBO7 compound. It can be thus concluded that alkoxy terminal chain length played the crucial role in the phase polymorphism of (*S*)-MHPSBO*n* compounds. From this series only the (*S*)-MHPSBO7 possesses rich phase polymorphism and in this subphases. It is probably caused by structural differences

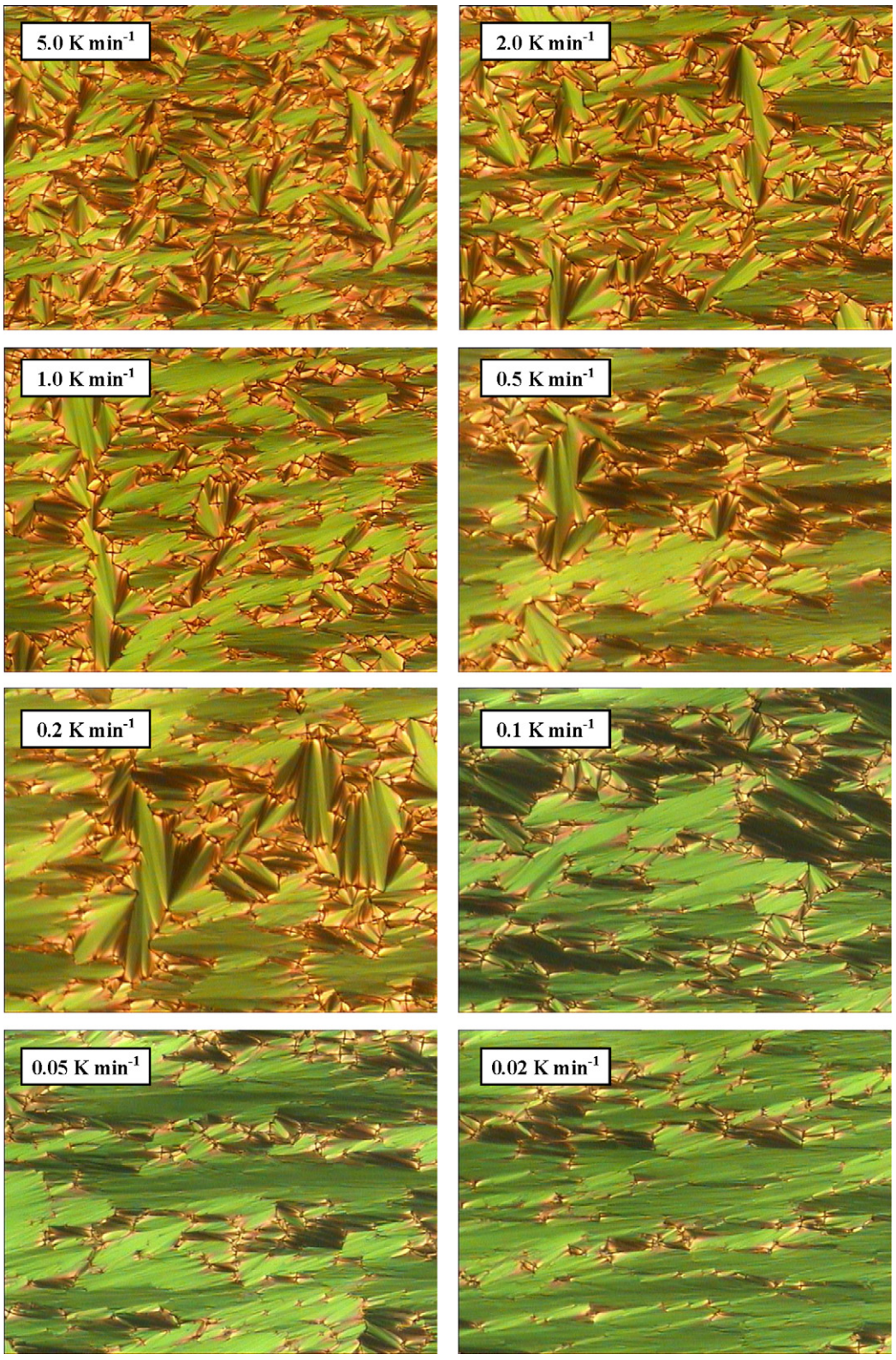

Fig. 7. Textures observed during cooling of the (*S*)-MHPSBO7 sample right behind I-SmA* phase transition (184.0 °C) for different cooling rates (from 5.0° min^{-1}, through 2.0° min^{-1}, 1.0° min^{-1}, 0.5° min^{-1}, 0.2° min^{-1}, 0.1° min^{-1}, 0.05° min^{-1} to 0.02° min^{-1}).

between these compounds in steric packing and the dipole interaction resulting from different lengths of terminal chain.

The DSC scan for (*S*)-MHPSBO7 that illustrates an especially important temperature region from 135 to 150 °C is presented in Fig. 4. It refers to heating and cooling (Fig. 4a and b respectively).

Phase transitions $SmC^*_A \leftrightarrow SmC^*_\gamma$, $SmC^*_\gamma \leftrightarrow SmC^*$, $SmC^* \leftrightarrow SmC^*_\alpha$ and $SmC^*_\alpha \leftrightarrow SmA^*$ have very low transition enthalpy (from 0.02 to 0.05 J g^{-1}, Table 1). These phase transitions are also well identified on the TLI curve (Fig. 5). On cooling of (*S*)-MHPSBO7, this phase sequence was deduced from the course of the TLI curve: I 187.5 °C

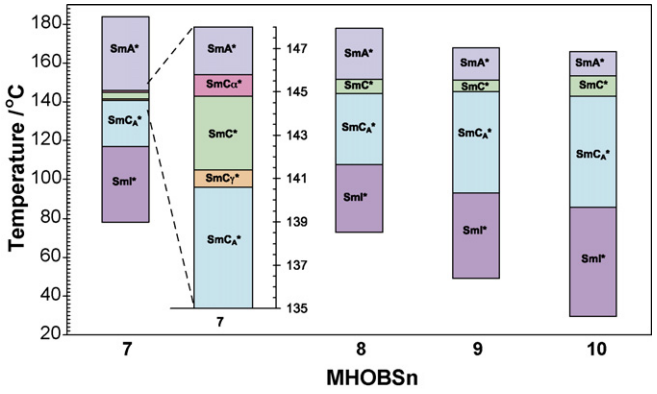

Fig. 8. Phase diagram for the (*S*)-MHPSBO*n* compounds obtained during cooling.

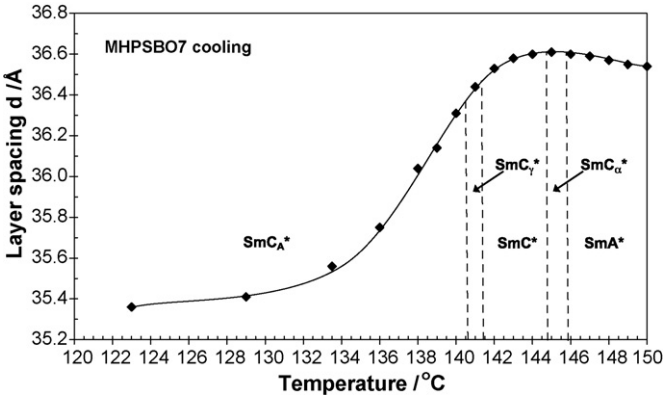

Fig. 9. Temperature dependence of layer spacing *d* for the (*S*)-MHPSBO7 compound obtained during cooling.

SmA*, 146.5 °C SmC^*_α, 145.2 °C SmC*, 141.3 °C SmC^*_γ, 140.6 °C SmC^*_A, 116.8 °C SmI*, 80.0 °C Cr. The transition temperatures between subphases and ferroelectric SmC* and antiferroelectric SmC^*_A phases were precisely determined on the basis of the first derivative of transmittance with respect to the temperature, calculated within the range of 139.0–148.0 °C. One can conclude that both DSC and TLI methods appear to be fruitful and complementary in establishing the phase sequence in liquid crystalline compounds.

Good experimental evidence has been obtained from the POM texture images of the (*S*)-MHPSBO7 sample for phase transitions from SmA* through subphase SmC^*_α ferroelectric SmC*, subphase SmC^*_γ and antiferroelectric SmC^*_A to Cr. The substance was placed in the cell identical to that used in TLI method (planar orientation). The microscope setting was kept unchanged while taking micrographs at different temperatures. However, the texture changes between phases are visible. Fig. 6 (Photo a) presents the I-SmA* phase transition. During cooling of the SmA* phase a fan shaped texture (Photo b) was found. This texture was changing upon further temperature decreasing and one could recognize characteristic textures of SmC^*_α, SmC*, SmC^*_γ, SmC^*_A and SmI* phases seen in Photos c, d, e, f, g (Fig. 6) respectively. Photo h presents the Cr phase.

The homogenization of the texture of the samples is the biggest problem in optical investigation. Fig. 7 presents the textures obtained during cooling of the (*S*)-MHPSBO7 sample right behind I-SmA* phase transition (184.0 °C) for different cooling rates. The last cooling rate was selected as an optimal rate and was applied to other substances.

From XRD and miscibility data the compounds (*S*)-MHPSBO7–(*S*)-MHPSBO10 have the enantiotropic SmC^*_A, SmC*, SmA* phases during heating and cooling and monotropic SmI* during cooling. Temperature ranges of the above-mentioned phases for all investigated compounds are presented in Fig. 8.

We can see that $\Delta T(SmC^*_A)$ for (*S*)-MHPSBO7, (*S*)-MHPSBO8, (*S*)-MHPSBO9 and (*S*)-MHPSBO10 possess a different range of the antiferroelectric SmC^*_A phase (phase diagram, Fig. 8). The increasing length of terminal alkoxy chain (from $n=7$ to 10) extends the mesophase range considerably during cooling ($\Delta T(SmC^*_A)=23.6$ and 61.8 °C for $n=7$ and 10 respectively).

The interlayer distances of chiral mesogens from the (*S*)-MHPSBO*n* homologous series were measured by means of X-ray diffraction as a function of temperature. The layer spacing *d* clearly decreases with lowering temperature in SmC* and subphase SmC^*_γ and antiferroelectric SmC^*_A. The biggest change is in SmC^*_A in the region of SmC^*_γ–SmC^*_A phase transition ((*S*)-MHPSBO7, from 36.28 Å at 141 °C to 35.84 Å at 138 °C). The minimal change was observed in subphase SmC^*_α and in SmC^*_α–SmC* phase transition. The change in the ferroelectric SmC* phase is similar to that in paraelectric SmA* (from 36.60 Å at 144.8 °C to 36.52 Å at 142.0 °C). The layer spacing *d* clearly decreases in proportion to the decreasing temperature in subphase SmC^*_γ as well as antiferroelectric SmC^*_A. The biggest change is noticeable in SmC^*_A phase (from 36.44 Å at 141.0 °C to 35.75 Å at 136.0 °C). Representative results for temperature dependence of the layer spacing *d* for ((*S*)-MHPSBO7 are given in Fig. 9.

The layer spacing *d* for the orthogonal SmA* phase for (*S*)-MHPSBO7 is equal to 36.57 Å in the vicinity of transition to SmC^*_α, at 145.8 °C. In the SmA* phase the layer spacing *d* is approximately 0.97 of the actual molecular length *l* (37.70 Å calculated by means of the semi-empirical MINDO3 method, it is not crystallographic data) in its fully extended conformations, including the covalent radii of the H atoms. The difference between *d* and *l* is probably caused by (*S*)-MHPSBO7 molecules being slightly tilted in SmA* phase which suggests that the SmA* phase can be of the de Vries type. Further other measurements are needed to study SmA*–SmC^*_α and SmC^*_α–SmC* phase transition.

The homogeneous textures were obtained during slow cooling (0.02 °C min^{-1}) from isotropic state to the SmA* phase. The optical observations and electro-optical studies have been carried out in the same conditions. Spontaneous polarization studies have been conducted using triangular field for all compounds from (*S*)-MHPSBO*n* homologous series. Temperature dependence of the spontaneous polarization value P_S for (*S*)-MHPSBO7 is presented in Fig. 10. The transition temperatures put in Fig. 10 were determined from DSC method.

A small value of spontaneous polarization is visible already at a temperature of over 155 °C degrees (SmA* phase). It is in

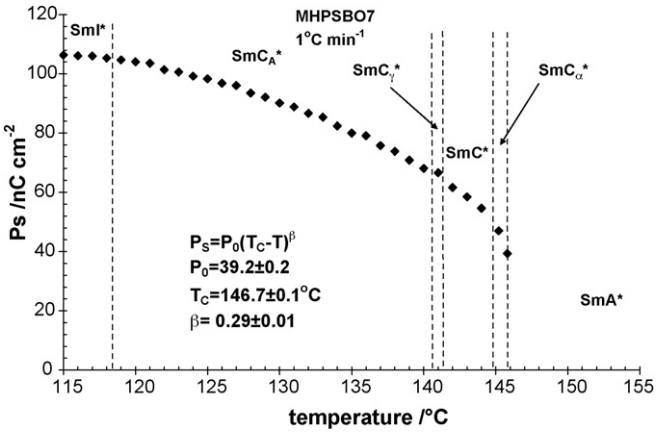

Fig. 10. Spontaneous polarization P_S for the (*S*)-MHPSBO7 compound vs. temperature obtained during cooling obtained at 10 Hz.

Table 2
Comparison of values of spontaneous polarization for compounds from (*S*)-MHPSBO*n* homologous series.

	Phase transitions	(*S*)-MHPSBO7	(*S*)-MHPSBO8	(*S*)-MHPSBO9	(*S*)-MHPSBO10
P	SmA*–SmC$^*_\alpha$	39.23	SmA*–SmC*	SmA*–SmC*	SmA*–SmC*
	SmC$^*_\alpha$–SmC*	45.35	23.49	28.90	34.59
	SmC*–SmC$^*_\gamma$	61.58	SmC*–SmC$^*_A$	SmC*–SmC$^*_A$	SmC*–SmC$^*_A$
	SmC$^*_\gamma$–SmC$^*_A$	66.60	69.86	107.53	110.90
	SmC$^*_A$–SmI*	105.33	136.11	162.16	182.02

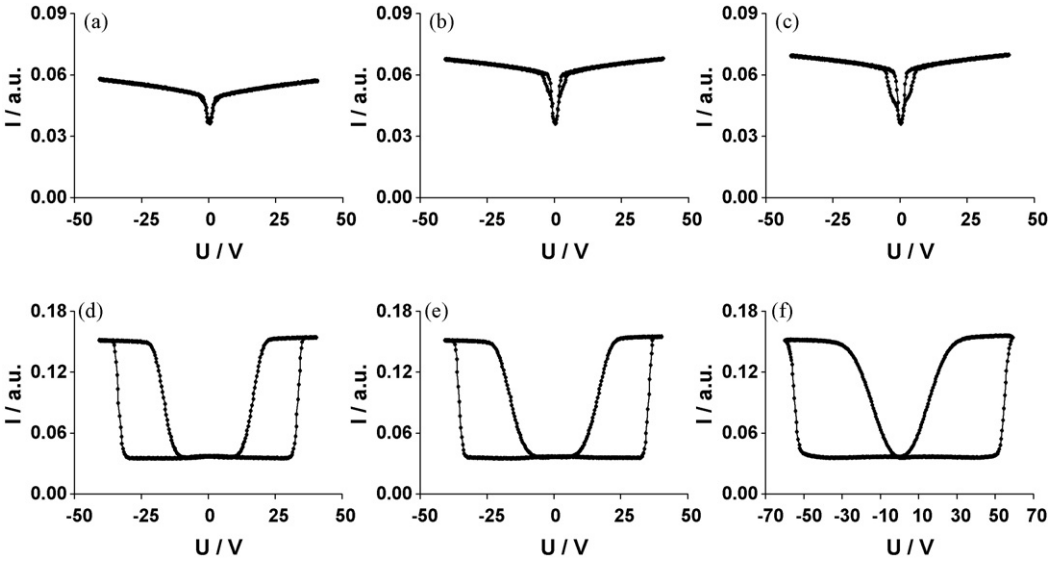

Fig. 11. Transmitted light curves vs. applied triangular-wave electric field of frequency 1 Hz and amplitude ±40 V/6.4 μm for the (*S*)-MHPSBO7 compound obtained during cooling: (a) at 145.3 °C (SmC$^*_\alpha$), (b) at 143.0 °C (SmC*), (c) at 141.0 °C (SmC$^*_\gamma$), (d) at 130.0 °C (SmC$^*_A$), (e) at 117.0 °C (SmI*) and (f) at 85.0 °C (SmI*).

accordance with tilt angle of molecules within the temperature range of SmA*–SmC$^*_\alpha$ phase transition (from ca. 10.0° at SmA*–SmC$^*_\alpha$ transition point to 0.0° at 155 °C in SmA* phase). The P_S values are 39.23, 45.35, 61.58, 66.60 and 105.33 nC cm^{-2} at the SmA*–SmC$^*_\alpha$, SmC$^*_\alpha$–SmC*, SmC*–SmC$^*_\gamma$, SmC$^*_\gamma$–SmC$^*_A$ and SmC$^*_A$–SmI* phase transitions respectively. Spontaneous polarization behaviour above 148.5 °C seems to be small, with a relatively high value of the spontaneous polarization close to 116.9 °C to SmC$^*_A$–SmI* phase transition. These thermal characteristics include a low temperature region which corresponds to the more orderly smectic phase (SmI* ≤ phase). Temperature dependence of the spontaneous polarization with theoretical fit is presented in Fig. 10. The equation describes changes of the spontaneous polarization between SmA*–SmC$^*_\alpha$ and SmC$^*_A$–SmI* phase transitions. The critical exponent obtained by fitting the square root law is equal to 0.37 and implies that changes of P_S values are increasing monotonic with decreasing temperatures. As there is a drop of the P_S values at the SmC$^*_A$–SmI* transition one can conclude that in this case a first order transition takes place. Similar results were earlier obtained for other compounds [32–34].

Between SmC$^*_\alpha$ subphase and ferroelectric SmC* phase, ferroelectric SmC* and SmC$^*_\gamma$ subphase as well as SmC$^*_\gamma$ subphase and antiferroelectric SmC$^*_A$ no distinct change of P_S value was observed. A comparison of P_S values between the homologous of (*S*)-MHPSBO*n* series is presented in Table 2 (P_S values were extrapolated at phase transition temperatures).

A similar characteristic of P_S values was observed for (*S*)-MHPSBO8, (*S*)-MHPSBO9 and (*S*)-MHPSBO10 in the region from SmC* to SmC$^*_A$. It seem to indicate that maximum of P_S values increasing with elongated of alkoxy terminal chain, from 105.33 nC cm^{-2} for (*S*)-MHPSBO7 to 182.02 nC cm^{-2} for (*S*)-MHPSBO10 at SmC$^*_A$–SmI* phase transition.

Optical transmittance vs. electric field (±60 V) was measured for (*S*)-MHPSBO*n* sample in 6.4 μm homogeneous cells at the frequency of 1.0 Hz of applied triangular-wave electric field. Some representative results obtained during cooling of the (*S*)-MHPSBO7 were presented in Fig. 11.

Small transmittance changes from 145.8 to 144.8 °C (SmC$^*_\alpha$, Fig. 11a) are visible. At a low frequency (1.0 Hz) the V-shaped switching was observed. Similar loops were observed in SmC$^*_\alpha$ for another compound [35]. The SmC$^*_\alpha$–SmC* phase transition at 144.8 °C was not observed as a considerable change in the characteristic shape of the switching pattern (Fig. 11b). A slight modulation of hysteresis loop was noticeable in the whole range of the SmC* phase. Similar changes were observed in SmC* for 10OPOSMH [17]. In the SmC$^*_\gamma$ a slight modulation of V-shaped switching was observed (Fig. 11c). In the antiferroelectric SmC$^*_A$ phase distinct changes in hysteresis loop were visible (Fig. 11d). The characteristic tristable switching pattern was observed in the whole temperature range of the antiferroelectric SmC$^*_A$ phase. The SmC$^*_A$–SmI* phase transition at 117 °C, i.e. exactly at the temperature of SmC$^*_A$–SmI* phase transition, was not observed as a considerable change in the tristable switching pattern (Fig. 11e). At a lower temperature the planar segment of the tristable switching becomes shorter during subsidence (Fig. 11f). This means that the molecule remained shorter in the anticlinic order. Other compounds from the (*S*)-MHPSBO*n* homologous series: (*S*)-MHPSBO8, (*S*)-MHPSBO9 and (*S*)-MHPSBO10 displayed identical behaviour.

4. Conclusions

A convenient preparation of new chiral of thiobenzoate ferroelectric–antiferroelectric liquid crystals, the (*S*)-MHPSBO*n* homologous series, is described. The (*S*)-MHPSBO7 possesses rich

phase polymorphism, including paraelectric SmA*, chiral ferroelectric SmC*, antiferroelectric SmC^*_A, monotropic SmI* phases and also smectic chiral subphases: SmC^*_α and SmC^*_γ. The higher homologoues have enantiotropic SmA*, SmC*, SmC^*_A and monotropic SmI* phases (for $n = 8–10$). The temperature range of the antiferroelectric SmC^*_A phase increases proportionally to the extending length of terminal alkoxy chain (for (*S*)-MHPSBO7 is equal to 23.6 °C and rises considerably and for (*S*)-MHPSBO10 is equal to 61.8 °C). The values of spontaneous polarization P_S in the ferroelectric SmC* phase changed in the range of 66.6–106.7 nC cm^{-2} and from 105.3 to 182.0 nC cm^{-2} in antiferroelectric SmC^*_A phase. These are relatively high values which may reveal possible application potential. Analysis of electro-optical switching properties of the SmI* phase leads to the conclusion that SmI* phase of (*S*)-MHPSBO*n* homologous series displays the behaviour typical of antiferroelectric phase.

Acknowledgements

The authors would like to thank Prof. Jan Przedmojski (Warsaw University of Technology, Poland) for X-ray measurements.

References

[1] A.D.L. Chandani, E. Górecka, Y. Ouchi, H. Takezoe, A. Fukuda, Jpn. J. Phys. 28 (1989) L1265.
[2] E. Górecka, A.D.L. Chandani, Y. Ouchi, H. Takezoe, A. Fukusa, Jpn. J. Appl. Phys. 29 (1990) 131.
[3] N. Okabe, Y. Suzuki, I. Kawamura, T. Isozaki, H. Takezoe, Jpn. J. Phys. 31 (1992) L793.
[4] I. Muševič, R. Blinc, B. Žekš, M. Čepič, M.M. Wittebrood, Th. Rasing, H. Orihara, Y. Ishibashi, Phys. Rev. Lett. 71 (1993) 1180.
[5] J. Philip, J.R. Lalanne, J.P. Marcerou, G. Sigaud, Phys. Rev. E 52 (1995) 1846.
[6] K. Ema, J. Watanabe, A. Takagi, H. Yao, Phys. Rev. E 52 (1995) 1216.
[7] M. Škarabot, M. Čepič, B. Žekš, R. Blinc, G. Heppke, A.V. Kityk, I. Muševič, Phys. Rev. 58E (1998) 575.
[8] E. Górecka, D. Pociecha, M. Čepič, B. Žekš, R. Dąbrowski, Phys. Rev. E 65 (2002) 061703.
[9] R.J. Twieg, K. Betterton, W. Hinsberg, P. Wong, W. Tang, H.T. Nguyen, Ferroelectrics 114 (1991) 295.
[10] W. Drzewiński, R. Dąbrowski, K. Czupryński, J. Przedmojski, M. Neubert, Ferroelectrics 212 (1998) 281.
[11] W. Drzewiński, K. Czupryński, R. Dąbrowski, J. Przedmojski, M. Neubert, S. Yakovenko, A. Murawski, Mol. Cryst. Liq. Cryst. 351 (2000) 297.
[12] R. Dąbrowski, Ferroelectrics 243 (2000) 1.
[13] M.E. Neubert, S.S. Keast, M.C. Ezenyilima, C.A. Hanlon, W.C. Jones, Mol. Cryst. Liq. Cryst. 237 (1993) 193.
[14] H.T. Nguyen, J.C. Rouillon, P. Cluzeau, G. Sigaud, C. Destrade, N. Isaert, Liq. Cryst. 17 (1994) 571.
[15] L. Nassifa, A. Jaklib, A.J. Seeeda, Mol. Cryst. Liq. Cryst. 365 (2001) 171.
[16] M.D. Ossowska-Chruściel, Liq. Cryst. 31 (2004) 1159.
[17] M.D. Ossowska-Chruściel, Phase Transitions 80 (2007) 757.
[18] M.D. Ossowska-Chruściel, Liq. Cryst. 34 (2007) 195.
[19] S. Zalewski, M.D. Ossowska-Chruściel, J. Chruściel, in: J. Chruściel, A. Szytuła, W. Zając (Eds.), Neutron Scattering and Complementary Methods in Investigations of Condensed Phase, vol. 2, Monograph No. 60, University of Podlasie Publishing House, Siedlce, 2005, p. 232.
[20] A. Filiks, M.D. Ossowska-Chruściel, J. Chruściel, in: J. Chruściel, A. Szytuła, W. Zając (Eds.), Neutron Scattering and Complementary Methods in Investigations of Condensed Phase, vol. 2, Monograph No. 60, University of Podlasie Publishing House, Siedlce, 2005, p. 246.
[21] M.D. Ossowska-Chruściel, J. Chruściel, S. Wróbel, Unpublished data (2009).
[22] M.D. Ossowska-Chruściel, S. Zalewski, A. Rudzki, A. Feliks, J. Chruściel, Phase Transitions 79 (2006) 679.
[23] M.D. Ossowska-Chruściel, P. Roszkowski, A. Rudzki, J. Chruściel, Liq. Cryst. 32 (2005) 877.
[24] J. Chruściel, B. Pniewska, M.D. Ossowska-Chruściel, Mol. Cryst. Liq. Cryst. 258 (1995) 325.
[25] Z. Karczmarzyk, M.D. Ossowska-Chruściel, J. Chruściel, Mol. Cryst. Liq. Cryst. 357 (2001) 117.
[26] M.D. Ossowska-Chruściel, Z. Karczmarzyk, J. Chruściel, Mol. Cryst. Liq. Cryst. 382 (2002) 37.
[27] K. Hori, S. Kawahara, K. Ito, Ferroelectrics 147 (1993) 91.
[28] K. Hori, K. Endo, Bull. Chem. Soc. Jpn. 66 (1993) 46.
[29] B. Jin, Z. Ling, Y. Takanishi, K. Ishikawa, H. Takezoe, A. Fukuda, M. Kakimoto, T. Kitazume, Phys. Rev. E 53 (1996) R4295.
[30] S. Yoshida, B. Jin, Y. Takanishi, K. Tokumaru, K. Ishikawa, T. Takezoe, A. Fukusa, T. Kusumoto, T. Nakai, S. Miyajima, J. Phys. Soc, Jpn. 68 (1999) 9.
[31] T. Nakai, S. Miyajima, Y. Takanishi, S. Yoshida, A. Fukusa, J. Phys. Chem. B 103 (1999) 406.
[32] M. Marzec, R. Dąbrowski, A. Fonfara, W. Haase, S. Hiller, S. Wróbel, Ferroelectrics 180 (1996) 127.
[33] S. Wróbel, M. Marzec, M. Godlewska, B. Gestblom, S. Hiller, W. Haase, Proc. SPIE 2372 (1995) 169.
[34] S. Hiller, A.M. Biradar, S. Wróbel, W. Haase, Phys. Rev. E 53 (1996) 641.
[35] P. Simeão Carvalho, M. Glogarova, M.R. Chaves, H.T. Nguyen, C. Destrade, J.C. Rouillon, S. Sarmento, M.J. Ribeiro, Liq. Cryst. 21 (1996) 511.